Quantitative analysis of dislocation arrangements induced by electromigration in a passivated Al (0.5 wt% Cu) interconnect

R. I. Barabash and G. E. Ice[a)]
Metals and Ceramics Divisions, Oak Ridge National Laboratory, Oak Ridge Tennessee 37831

N. Tamura
Advanced Light Source, 1 Cyclotron Road, Berkeley, California 94720

B. C. Valek and J. C. Bravman
Department of Materials Science & Engineering, Stanford University, Stanford, California 94305

R. Spolenak
Max Planck Institut für Metallforschung, Heisenbergstrasse 3, D-7056 Stuttgart, Germany

J. R. Patel
Advanced Light Source, 1 Cyclotron Road, Berkeley, California 94720 and Stanford Synchrotron Radiation Laboratories, P.O. Box 4349, Stanford, California 94309

(Received 14 October 2002; accepted 3 February 2003)

Electromigration during accelerated testing can induce plastic deformation in apparently undamaged Al interconnect lines as recently revealed by white beam scanning x-ray microdiffraction. In the present article, we provide a first quantitative analysis of the dislocation structure generated in individual micron-sized Al grains during an *in situ* electromigration experiment. Laue reflections from individual interconnect grains show pronounced streaking during the early stages of electromigration. We demonstrate that the evolution of the dislocation structure during electromigration is highly inhomogeneous and results in the formation of unpaired randomly distributed dislocations as well as geometrically necessary dislocation boundaries. Approximately half of all unpaired dislocations are grouped within the walls. The misorientation created by each boundary and density of unpaired individual dislocations is determined. The origin of the observed plastic deformation is considered in view of the constraints for dislocation arrangements under the applied electric field during electromigration. © *2003 American Institute of Physics.*
[DOI: 10.1063/1.1563033]

I. INTRODUCTION

During service, the tiny Al or Cu metallic interconnect lines (width in the micron and submicron range) which connect discrete components in modern integrated circuits, experience extremely high current densities on the order of 1 MA/cm^2. The so-called electron ''wind'' force is sufficient to ''physically'' displace the constitutive atoms in the interconnect lines. This phenomenon, called electromigration, depletes material at the cathode end of the interconnect line and cause accumulation near the anode end.[1] Ultimately electromigration leads to failure by open (void formation) or short (cracking of the passivation layer and material extrusion) circuit. Electromigration-induced failure in metal interconnect constitutes a major and growing reliability problem in the semiconducting industry.[2] While the general mechanism of electromigration is understood,[3] the effect of the atomic flow on the local metallic line microstructure is largely unknown, specifically in the early stages of electromigration.

Recently, experimental techniques capable of probing grain orientation and stress with a spatial resolution compatible with the dimensions of the lines have emerged.[4–12] For example, intense x-ray white or monochromatic microbeams produced at third-generation synchrotron sources can probe local microstructure (grain orientation as well as local strain/stress tensors) with submicron spatial resolution. White-beam x-ray microdiffraction using Kirkpatrick–Baez mirror focusing optics and a large area charge-coupled-device (CCD) detector[4–8] is particularly well suited to the study of electromigration because it allows for rapid measurement of elastic and plastic deformation tensors with crystallographic orientation and boundary conditions. In these measurements white-beam microdiffraction was applied to spatially resolved stress studies of polycrystalline thin films during *in situ* conditions.[5–7] The technique was used to probe microstructure in interconnects[4,13–16] and recently unambiguously unveiled the plastic nature of the deformation induced by mass transport during electromigration in Al(Cu) lines[17] even before macroscopic damage occurred. Pioneering work on Al electromigration studied with a 10 μm white beam and an energy dispersive detector has also been previously performed by Wang *et al.*[12]

New analysis methods are currently being developed to quantify the observed deformation from x-ray microdiffraction studies. The method for the analysis of dislocation networks described in this paper, together with rocking curve,[18] ultra-small-angle x-ray scattering[19] and transmission electron

[a)]Electronic mail: barabashr@ornl.gov

 © 2003 American Institute of Physics

Downloaded 04 Sep 2009 to 160.91.157.167. Redistribution subject to AIP license or copyright; see http://jap.aip.org/jap/copyright.jsp

microscopy (TEM) (Refs. 20 and 21) methods reveal different features of dislocation arrangement. Grain-scale heterogeneity of plastic strain in polycrystalline Al was analyzed by continuum finite element simulations and compared with electron back scattering results.[22] The aim of the present article is to understand the complex dislocation structure arising from electromigration-induced plastic deformation by simulating the shape of the reflections observed in the experimental data. Custom software allows us to determine the orientation of the predominant dislocation network in each sample subgrain.[23,24]

II. EXPERIMENT AND ANALYSIS

Data collections have been carried out on the x-ray microdiffraction end station (7.3.3.) at the Advanced Light Source. The sample is a patterned Al(0.5 wt % Cu) line (length:30 μm, width 4.1 μm, thickness 0.75 μm) sputter deposited on a Si wafer and buried under a glass passivation layer (0.7 μm thick). Electrical connections to the line are made through unpassivated Al(Cu) pads connected to the sample by W vias. The sample was maintained at a constant temperature of 205 °C and the current density was progressively ramped up to 0.98 MA/cm^2 and maintained at this value for a period of 11 h. The direction of the current was then reversed for a total period of 19 h. Before and during the course of electromigration, the sample was repeatedly raster scanned under a micron-size white beam with a step size of 0.5 μm. At each step, a CCD diffraction frame was collected. Each scan contains 975 frames covering the total surface of the sample. In the present article, we concentrate on the evolution of the diffraction pattern of one particular grain (grain A, size: ~2.5 μm) situated approximately half way between the middle of the line and the anode end. Details on the experimental setting and data collection can be found elsewhere.[4–6] A qualitative description and semiquantitative interpretation of the entire data set collected for the present sample will be published in a forthcoming paper.[17] Orientation maps obtained from the x-ray microdiffraction scans reveal that the grain structure of the line has a random in-plane orientation and pronounced (111) fiber texture. Only one or a few grains span the line (near bamboo configuration). Grain A is in a region of the line, where multiple grains are found transverse to the line.

The white beam CCD frames show sharp Laue reflection before electromigration and pronounced streaking of the Laue reflections in the majority of Al grains after electric current flow (Fig. 1). The average streaking direction is approximately transverse to the length of the line (and not along the line). Intensity distributions along the streak direction (ξ) are typically nonuniformly bunched into several maxima indicating that the dislocation distribution is inhomogeneous. Large intergranular and intragranular stress variations have been measured in similar samples.[4,16] They indicate, that local parameters such as grain orientation, grain initial stress, grain size, and type of grain boundaries play a crucial role in understanding the coupling between inhomogeneous plastic deformation of polycrystalline thin film and electromigration.

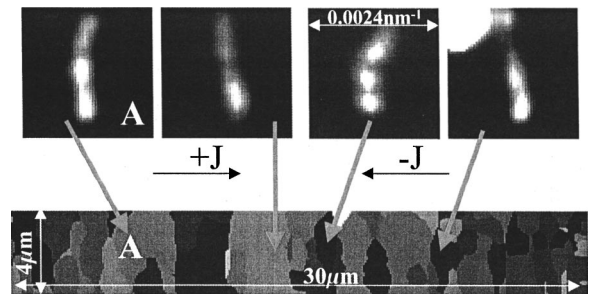

FIG. 1. Experimental streaking of Laue images for different grains of interconnect line in a polycrystalline region. The side of each Laue spot insets is 0.0024 nm^{-1} (images were converted from angular units to nm^{-1}). The spatial length scale is given by the line dimensions: 4.1 μm in width and 30 μm in length.

The dislocation structure was analyzed based on the approach described by Barabash *et al.*[23,24] Here, we extended the method to consider individual unpaired dislocations [geometrically necessary dislocations (GNDs)] within the scattering domains separated by geometrically necessary dislocation boundaries (GNB).

Consider a net of individual unpaired edge dislocations with a density n^+ within a scattering domain (Fig. 2). All dislocations from this set have Burgers vectors, $\mathbf{b_i}$ and dislocations lines $\boldsymbol{\tau}$. We introduce a coordinate system with the X axis in the direction of the Burgers vector and the Z axis in the direction of the dislocation line. Each edge dislocation at a position labeled t in the XY plane creates a displacement $\mathbf{u}_{it}$ of the ith scattering cell in that plane. The projections of the displacement vector in this plane for the simple case of elastically isotropic crystals, are described by the following equations:[25,26]

$$u_x=\frac{b}{2\pi}\left[\tan^{-1}\frac{y}{x}+\frac{xy}{2(1-\mu)(x^2+y^2)}\right],$$
$$u_y=-\frac{b}{2\pi}\left[\frac{1-2\mu}{2(1-\mu)}\ln(x^2+y^2)+\frac{(x^2-y^2)}{4(1-\mu)(x^2+y^2)}\right], \quad (1)$$

where μ is the Poisson's ratio and b the length of the Burgers vector. The total displacement of the ith cell $\mathbf{u}_i$ is due to all dislocations and is defined by the equation:

$$\mathbf{u}_i=\sum_t c_t\mathbf{u}_{it}. \quad (2)$$

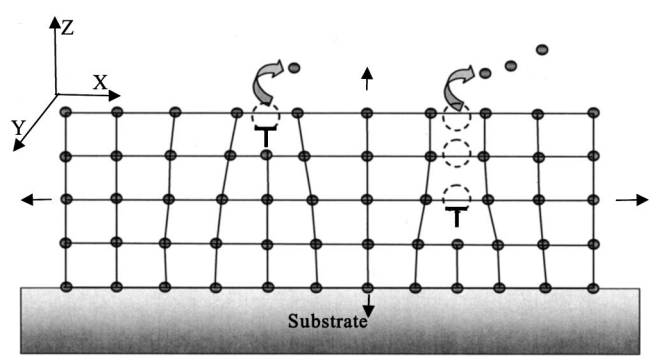

FIG. 2. Scheme of dislocation climb and formation of vacancies during electromigration.

Downloaded 04 Sep 2009 to 160.91.157.167. Redistribution subject to AIP license or copyright; see http://jap.aip.org/jap/copyright.jsp

To describe the distribution of dislocations belonging to the set in a given XY plane, we introduce the number c_t. It can take two values:

$$c_t = \begin{cases} 1, & (+) \\ 0, & (-). \end{cases} \tag{3}$$

If there is a dislocation in the position t, the corresponding number $c_t = 1$, and in positions without dislocations $c_t = 0$. The difference between displacements of two scattering lattice cells i and j can be written as[23,27]

$$\mathbf{u}_{it} - \mathbf{u}_{jt} = (\mathbf{R}_{ij}\nabla)\mathbf{u}_{it} + \frac{1}{2}(\mathbf{R}_{ij}\nabla)^2\mathbf{u}_{it}, \quad \text{with} \quad \nabla \equiv \nabla_{R_i}. \tag{4}$$

For unpaired dislocations, the mean deformation tensor $\hat{\omega}^r$ can be written in terms of the antisymmetric Levi–Civita tensor of third rank $\epsilon_{\tau lm}$ and a dislocation density tensor of second rank $\rho_{\tau n}$:[23,25]

$$\epsilon_{\tau lm}\left(\frac{\partial \omega_{mn}}{\partial x_l}\right) = -\rho_{\tau n}. \tag{5}$$

There are only two non-zero components of the mean deformation tensor $\hat{\omega}^r$ for our net of parallel unpaired dislocation:

$$\omega^r_{xy} = -\omega^r_{yx} = n^+ bx. \tag{6}$$

This distortion field represents a pure rotation about the Z axis that increases with displacement in x.

To take into account the presence of geometrically necessary tilt boundaries we consider several GNBs formed by walls of edge dislocations. Following the classification in Refs. 20, 21, and 25 we can distinguish between incidental dislocation boundaries (IDBs) forming cell boundaries due to mutual trapping of glide dislocations from geometrically necessary boundaries (GNBs). According to Raabe *et al.*[22] in pure Al GNBs separate volume elements where different slip systems are activated, or having different strain tensor components. We assume that GNBs are formed due to partial grouping of individual GNDs into the wall and that the type of dislocations within the scattering domain is the same as within the wall. Such a wall provides a rotation between two neighboring domains around the direction of dislocation lines within the wall. The unit vector $\boldsymbol{\omega}$ parallel to the rotation axis of each wall coincides with the unit vector $\boldsymbol{\tau}$ along the dislocation lines in the case of a tilt boundary. We consider pure tilt boundaries formed by equidistant edge dislocations (so called "thin walls"[18]). Such boundaries do not produce long-range strain, only rotations. The residual stresses in the boundary region are periodic with a wavelength

$$b^* = b \operatorname{cosec} \Theta/2. \tag{7}$$

These stresses are appreciable only at the distances less then b^* from the boundary.[25] If h is the distance between these dislocations in the wall, one can consider the boundary as a single defect producing the local rotation field. The misorientation angle Θ due to such a boundary is defined by the equation

$$b/h = 2\sin(\Theta/2), \tag{8}$$

where $b/h \approx \Theta$ for small angle boundaries. To characterize this model quantitatively, we define the average size of the scattering domain D between the two neighboring GNBs and write the number of walls per unit length as $1/D$. The total density of unpaired dislocations grouped in the walls is denoted by

$$n^w = \frac{1}{Dh}. \tag{9}$$

The mean deformation tensor ω^w-due to the presence of GNBs results in pure rotations about the direction of dislocation lines in the wall. For the orientation of the dislocations within a wall described above, an axis X is perpendicular to the plane of the wall, and an axis Z parallel to the direction of dislocation lines in the wall. For this coordinate system, two nonzero components of the mean deformation tensor are equal because of the wall and are defined by

$$\omega^w_{xy} = -\omega^w_{yx} = \Theta x/D. \tag{10}$$

This tensor depends on the type and misorientation angles of each GNB and their number. Local lattice rotation fields from individual dislocations and GNBs superimpose and the mean distortion field tensor can be written as follows:

$$\omega_{xy} = \omega^w_{xy} + \omega^r_{xy}. \tag{11}$$

In general, the orientation of dislocations within the boundary may not coincide with the orientation of dislocations within the scattering domain and a more general consideration must be used.

Near a Laue reflection, we can define two natural axes ξ and v in the plane perpendicular to the momentum transfer unit vector $\mathbf{g}$. As in Refs. 23 and 24 with this coordinate system, the diffuse scattering is strongly elongated in the ξ direction. The full width at half maximum in the ξ direction, FWHM_ξ, depends on the average distance between GNBs, their mutual orientation with the momentum transfer $\mathbf{G}$, the type of GNB (tilt or twist), and the incident x-ray beam direction. In the second transverse direction v, the FWHM_v depends on the total number of boundaries per unit length b/D and usually $\mathrm{FWHM}_v \ll \mathrm{FWHM}_\xi$.

Reciprocal space projections of all (111) Laue spots were recovered from experimental data. The intensity profiles along the streak at different times during the electromigration process are presented in Fig. 3(a) for grain A in the reciprocal space. Continuous streaks are observed near all Laue spots in the first measurements made at 0.98 MA/cm^2 [Fig. 3(b), curve 1]. The full width at half maximum (FWHM_ξ) along the streak direction increased almost twice relatively to the initial (no current) state [Fig. 3(a), curve 2]. The highly asymmetric shape of the intensity profile along the streak indicates that the arrangement of unpaired dislocations is inhomogeneous. The orientation of the primary unpaired (geometrically necessary) dislocations (GND) corresponds to a Burgers vector $\mathbf{b}=[0\text{–}11]$ and a dislocation line direction $\tau=[2\text{-}1\text{-}1]$. The density of unpaired dislocations is equal to $n^+ = 0.3\times 10^{10}\,\mathrm{cm}^{-2}$ (Fig. 4), which is a quite reasonable value for plastically deformed Al. After six additional hours at the same current density, the intensity distribution breaks into two distinct maxima (Fig. 3, curve 3)

Downloaded 04 Sep 2009 to 160.91.157.167. Redistribution subject to AIP license or copyright; see http://jap.aip.org/jap/copyright.jsp

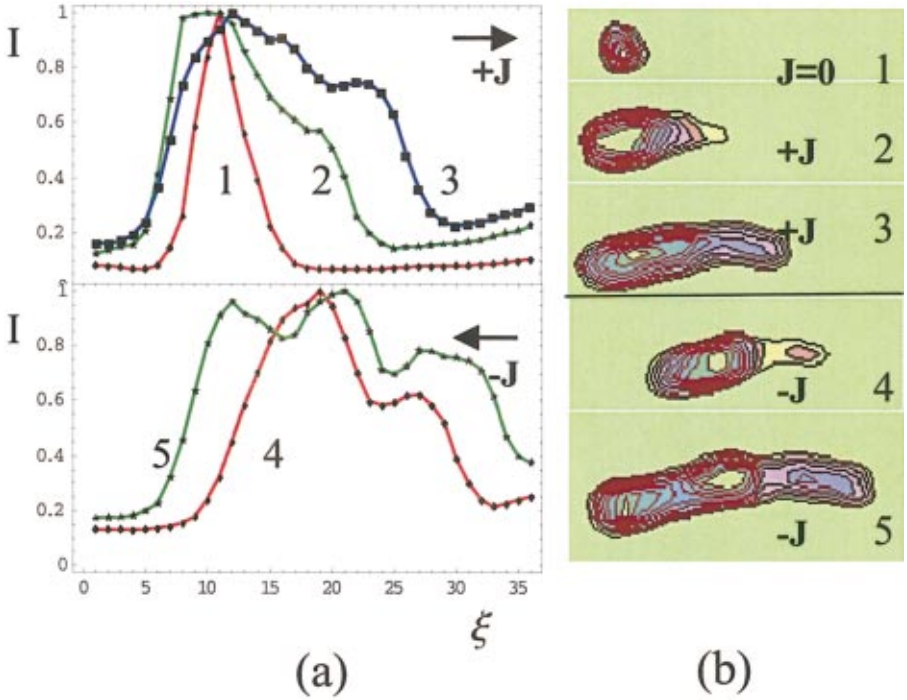

FIG. 3. (Color) Intensity distribution along the streak of the (222) reflection (a) and their contourmaps (b) in the reciprocal space: (1) at 205 °C without current flow; (2) flow $J=+0.98\ \mathrm{MA/cm^2}$ during 14 h; (3) flow $J=+0.98\ \mathrm{MA/cm^2}$ during 20 h; (4) flow $J=-0.98\ \mathrm{MA/cm^2}$ during 36 h; and (5) flow $J=-0.98\ \mathrm{MA/cm^2}$ during 46 h.

indicating that the dislocation structure partially relaxed with the formation of a geometrically necessary boundary. The misorientation created by this boundary is ~0.38°. The average distance between the boundary dislocations within the wall is estimated to be 430 Å. The density of boundary dislocations is about $0.3\times10^{10}\ \mathrm{cm^{-2}}$. The FWHM_ξ along the streak direction within each maximum again increased [Fig. 3(a), curve 3]. The density of unpaired individual dislocations within each scattering domain at this stage is equal to $n^+=0.5\times10^{10}\ \mathrm{cm^{-2}}$ (Fig. 4).

We then reversed the direction of the current flow to $-0.98\ \mathrm{MA/cm^2}$, and after 6 h the total FWHM_ξ of the streak decreases slightly (Fig. 3, curve 4). This indicates that the opposite direction of the current may "cure" some part of randomly distributed unpaired individual dislocations. The density of unpaired individual dislocations within each scattering domain slightly decreases to $n^+=0.4\times10^{10}\ \mathrm{cm^{-2}}$. However, the dislocations being grouped into a sub-boundary form a very stable arrangement, which are not destroyed by the opposite direction of the current. Its misorientation remains practically the same as in previous stage boundary and is equal to 0.38°. After 10 h with $J=-0.98\ \mathrm{MA/cm^2}$ a second sub-boundary with $\mathbf{b}=[110]$, $\tau=[-112]$ is generated. The FWHM_ξ of the streak again almost doubled and three distinct maxima are observed (Fig. 3, curve 5). The second geometrically necessary boundary creates misorientation of 0.52° around the $[\bar{1}12]$ axes. The average distance between the boundary dislocations within the wall decreases to 315 Å. The total density of boundary dislocations within the above two boundaries is equal to $0.7\times10^{10}\ \mathrm{cm^{-2}}$. Approximately half of all unpaired dislocations remain randomly distributed within the three fragments with a density of $0.7\times10^{10}\ \mathrm{cm^{-2}}$. Various intensity contour maps during electromigration are shown at Fig. 3(b). We have simulated the Laue images (contourmaps) corresponding to the experimental dislocation arrangements. In Fig. 5, the best fits are shown for the (222) simulated and experimental contour maps (a) and their corresponding intensity profiles along the streak.

III. DISCUSSION

Our analysis of the orientation of the activated dislocation slip systems shows that the slip systems with dislocation lines almost parallel to the direction of current flow are activated first (although this is not intuitive).

While the possibility of plastic yield during electromigration has been considered in the literature,[3] a direct quantitative analysis of the dislocation formation during electromigration is performed here for the first time. According to Refs. 3, 12, and 16, interconnect lines develop residual stress during manufacturing. However, the local stress distribution is highly inhomogeneous.[5,16] During electromigration the observed atomic flux is accompanied by vacancy and void fluxes and a stress gradient developed along the inter-

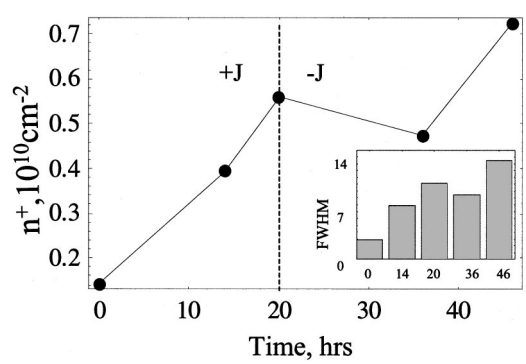

FIG. 4. Change of unpaired dislocation density n^+ and FWHM (inset) during electromigration.

Downloaded 04 Sep 2009 to 160.91.157.167. Redistribution subject to AIP license or copyright; see http://jap.aip.org/jap/copyright.jsp

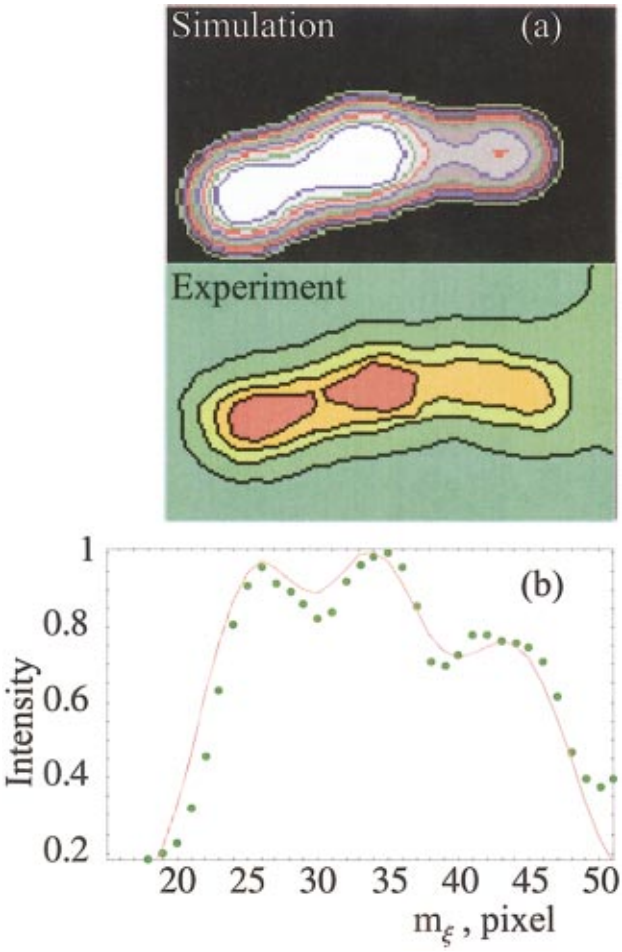

FIG. 5. (Color) Simulated (top) and experimental (bottom) images of the (222) Laue images (a) and their corresponding intensity profiles along the streak (dots, experimental data; solid line, simulation) (b). The simulation was performed with two activated dislocation systems grouped into tilt walls: $b=[0-11]$, τ=[2-1-1] and $b=[110]$, τ=[−112].

connect line. The larger Cu atoms (0.5 wt %) suppress diffusion of the host Al atoms and increase the lifetime of interconnects. Due to different bulk and surface diffusion coefficients the various fluxes change near the surface. The whole process of electromigration is thought to depend on the conditions for the creation and annihilation of vacancies in the grain. The ratio between the average distance l between the sources and sinks of vacancies in comparison with the effective length L where concentration gradients of atoms and vacancies may be considered constant is one of the important parameters. If $l \ll L$, the vacancy and atomic gradients are linearly related. If $l \sim L$ or $l > L$ the vacancy and atomic gradients may be considered independent. It results in a different behavior of small and large grains of the interconnect line during electromigration, as observed experimentally,[17] small grains rotate as a whole and large grains show intensive formation of dislocations. Dislocation climb during electromigration becomes the main mechanism of stress relaxation and the source of vacancies (Fig. 2). Alloying effects in electromigration were also considered in details.[28,29] The osmotic force per unit length applied to the climbing dislocation is equal to[30]

$$F_z^{\mathrm{osm}} = -\frac{kTb}{v}\ln\frac{c}{c_0}, \tag{12}$$

and depends on the ratio between the real vacancy concentration c near a dislocation and equilibrium concentration c_0. Here, k is the Boltzman's constant and T is the temperature. The total force per unit length of the dislocation is equal to

$$F = \sigma_{xx} b - \frac{kTb}{v}\ln\frac{c}{c_0}, \tag{13}$$

where σ_{xx} is the stress component across the direction of the interconnect line. The relative density change dc/c in the vicinity of climbing dislocation results in a stress value increment:[3]

$$\frac{dc}{c} = -\frac{d\sigma}{B}.$$

Here, B is a coefficient which depends only on the elastic properties of the aluminum and silicon and on the aspect ratio between the thickness and the width of the interconnect line. For aluminum lines on a silicon substrate, coefficient $B=(0.5\text{–}0.75)G$, where G is the Young's modulus for aluminum.

Reversal of the current flow partially cures randomly distributed dislocations, however, stable dislocation walls configurations are not destroyed by the current reversal.

The elastic field around climbing dislocations generates an elastic field through the entire crystal (grain), which interacts with phonons in the crystal (phonon viscosity)[31] as well as with electrons. Dislocations and dislocation walls scatter electrons off the initial direction by the deformation potential related to them. The major contribution to the interaction potential between electrons and dislocations comes from the deformation field in the matrix around the dislocation, and not from the dislocation core. Around an edge dislocation the deformation field decreases very slowly, as $1/r_\perp$ ($r_\perp$ is the distance to the dislocation line), leading to a large scattering matrix element. However, scattering only occurs in the direction perpendicular to the dislocation line, because of translation invariance along the dislocation line. The scattering of the electrons can be described as

$$(\boldsymbol{k}_0 - \boldsymbol{k})\tau = 2\pi n/d_{\tau-}, \quad n = 0, +(-)1\cdots. \tag{14}$$

Here, d_τ is a lattice parameter along the dislocation line τ and $\boldsymbol{k}_0$, $\boldsymbol{k}$ are wave vectors of incident and scattered electrons. There exists a strong anisotropy of scattering. The probability of scattering depends on the difference $(\boldsymbol{k}_0 - \boldsymbol{k})$ as well as on the direction of initial electron momentum $\boldsymbol{k}_0$. When almost all unpaired dislocations with the density n^+ are parallel (as in the case of Al-based interconnects) the anisotropy of scattering becomes important and the electrical properties of the interconnect depend strongly on the direction of the electric current relative to the orientation of the dislocation network. The electron's scattering time in the presence of a parallel set of edge dislocations with density n^+, can be estimated as follows:[31]

$$\frac{1}{\tau(k)} = n^+ v_\perp s. \tag{15}$$

Downloaded 04 Sep 2009 to 160.91.157.167. Redistribution subject to AIP license or copyright; see http://jap.aip.org/jap/copyright.jsp

Here, $\tau(k)$ is the time between large angle scattering events of the electron, $v_{\perp}$ is the transverse component of the velocity, s is the linear scattering cross section. The energy loss due to scattering can be estimated as $Q \sim 1/\tau(k)$. The largest scattering occurs in the plane transverse to the dislocation line. In our measurements dislocations are formed in thin Al-based interconnects under the applied electric field during electromigration. The applied electric field creates additional constraints for dislocations. If a dislocation is formed with the line perpendicular to the applied electric field, scattering of electrons leads to the increased local Joule heating, and such dislocation will be more likely to anneal. On the other hand, a dislocation network with the lines close to the direction of the electric current creates the smallest resistance for the electric current, and is therefore more likely to persist.

A rough estimate shows that for a dislocation density of $0.5\times 10^{10}\,\mathrm{cm}^{-2}$, as determined in our experiments, and for a current flow of 1 MA in the Al(0.5 wt% Cu) interconnect line, a change in orientation of the dislocations from parallel to perpendicular to the current flow direction, creates additional resistivity and causes additional heat dissipation of about $25\ \mathrm{j\,s}^{-1}$ per unit length of the dislocation line resulting in the increase of local temperature with the rate of $8\ \mathrm{K\,s}^{-1}$ in the region surrounding the dislocation core within the scattering cross section. This heat is larger than the one estimated from thermal conductivity through the cylindrical surface surrounding the dislocation core. As a result the dislocations with line with the smallest angle to the current flow are formed first. When the above slip planes saturate the next possible slip system is activated which has the next smallest inclination angle to the current direction.

Although the field of polychromatic microdiffraction is still very young, it is clear that white-beam x-ray microdiffraction is able to provide quantitative information about unpaired dislocation density and structure hierarchy and gives the parameters for the dislocation population within the geometrically necessary boundary. This kind of analysis as a function of grain orientation and local stress is essential to improve our understanding of the effects of local microstructure on electromigration induced deformation in interconnects and can be used to predict the properties of materials under constraints.

ACKNOWLEDGMENTS

Research is supported by the Director, Office of Science, Office of Basic Energy Sciences, U.S. Department of Energy, under Contract, No. DE-AC05-00OR22725 with UT-Battelle, LLC and with the Advanced Light Source, Materials Science Division, under the Contract No. DE-AC03-76SF00098 at Lawrence Berkeley National Laboratory.

[1] I. A. Blech, J. Appl. Phys. **47**, 1203 (1976).
[2] C. V. Thompson and J. R. Lloyd, Mater. Res. Bull. **18**, 19 (1993).
[3] M. A. Korhonen, P. Borgesen, K. N. Tu, and C.-Y. Li, J. Appl. Phys. **73**, 3790 (1993).
[4] N. Tamura, A. A. MacDowell, R. S. Celestre, H. A. Padmore, B. C. Valek, J. C. Bravman, R. Spolenak, W. L. Brown, T. Marieb, H. Fujimoto, B. W. Batterman, and J. R. Patel, Appl. Phys. Lett. **20**, 3724 (2002).
[5] N. Tamura, R. Spolenak, B. C. Valek, A. Manceau, M. Meier Chang, R. S. Celestre, A. A. MacDowell, H. A. Padmore, and J. R. Patel, Rev. Sci. Instrum. **73**, 1369 (2002).
[6] A. A. MacDowell, R. S. Celestre, N. Tamura, R. Spolenak, B. C. Valek, W. L. Brown, J. C. Bravman, H. A. Padmore, B. W. Batterman, and J. R. Patel, Nucl. Instrum. Methods Phys. Res. A **467-468**, 936 (2001).
[7] G. E. Ice and B. C. Larson, Adv. Eng. Mater. **2**, 643 (2002).
[8] B. C. Larson, Wenge Yang, G. E. Ice, J. D. Budai, and J. Z. Tischler, Nature (London) **415**, 887 (2002).
[9] L. Margulies, G. Winther, and H. F. Poulsen, Science **291**, 2392 (2001).
[10] J. S. Chung and G. E. Ice, J. Appl. Phys. **86**, 5249 (1999).
[11] P.-C. Wang, I. C. Noyan, S. K. Kaldor, J. L. Jordan-Sweet, E. G. Liniger, and C.-H. Ku, Appl. Phys. Lett. **78**, 2712 (2001).
[12] P. C. Wang, G. S. Cargill III, I. C. Noyan, and C. K. Hu, Appl. Phys. Lett. **72**, 1296 (1998).
[13] N. Tamura, J.-S. Chung, G. E. Ice, B. C. Larson, J. D. Budai, J. Z. Tischler, M. Yoon, E. L. Williams, and W. P. Lowe, Mater. Res. Soc. Symp. Proc. **563**, 175 (1999).
[14] N. Tamura, B. C. Valek, R. Spolenak, A. A. MacDowell, R. S. Celestre, H. A. Padmore, W. L. Brown, T. Marieb, J. C. Bravman, B. W. Batterman, and J. R. Patel, Mater. Res. Soc. Symp. Proc. **612**, D.8.8.1 (2001).
[15] R. Spolenak, D. L. Barr, M. E. Gross, K. Evans-Lutherodt, W. L. Brown, N. Tamura, A. A. MacDowell, R. S. Celestre, H. A. Padmore, J. R. Patel, B. C. Valek, J. C. Bravman, P. Flinn, T. Marieb, R. R. Keller, and B. W. Batterman, Mater. Res. Soc. Symp. Proc. **612**, D10.3.1 (2001).
[16] B. C. Valek, N. Tamura, R. Spolenak, A. A. MacDowell, R. S. Celestre, H. A. Padmore, J. C. Bravman, B. W. Batterman, and J. R. Patel, Mater. Res. Soc. Symp. Proc. **673**, P7.7.1 (2001).
[17] B. C. Valek, N. Tamura, R. Spolenak, J. C. Bravman, A. A. MacDowell, R. S. Celestre, H. A. Padmore, W. L. Brown, B. W. Batterman, and J. R. Patel, Appl. Phys. Lett. **81**, 4168 (2002).
[18] H. Trenkler, R. Barabash, H. Dosch, and S. C. Moss, Phys. Rev. B **64**, 214101 (2001).
[19] G. G. Long, L. E. Levine, and R. Thomson, J. Appl. Crystallogr. **33**, 456 (2000).
[20] D. Hughes and N. Hansen, Acta Mater. **48**, 2985 (2000).
[21] Q. Liu, D. J. Jensen, and N. Hansen, Acta Mater. **46**, 5819 (1998).
[22] D. Raabe, M. Sachtleber, R. Zhao, F. Roters, and S. Zaefferer, Acta Mater. **49**, 3433 (2001).
[23] R. Barabash, G. E. Ice, B. C. Larson, G. M. Pharr, K.-S. Chung, and W. Yang, Appl. Phys. Lett. **79**, 749 (2001).
[24] R. Barabash, G. E. Ice, B. C. Larson, and W. Yang, Rev. Sci. Instrum. **73**, 1652 (2002).
[25] M. Wilkens, T. Ungar, and H. Mughrabi, Phys. Status Solidi A **104**, 157 (1987).
[26] F. R. N. Nabarro, *Theory of Crystal Dislocations* (Dover, New York, 1987).
[27] M. A. Krivoglaz, *Theory of X-Ray and Thermal Neutron Scattering by Real Crystals* (Plenum, New York, 1969).
[28] R. Spolenak, O. Kraft, and E. Arzt, AIP Conf. Proc. **491**, 126 (1999).
[29] C. Witt, C. Volkert, and E. Arzt, Acta Mater. **51**, 49 (2003).
[30] J. P. Hirth and J. Lothe, *Theory of Dislocations* (Wiley, New York, 1982).
[31] J. Ziman, *Electrons and Phonons* (Clarendon, Oxford, 1962).

Downloaded 04 Sep 2009 to 160.91.157.167. Redistribution subject to AIP license or copyright; see http://jap.aip.org/jap/copyright.jsp